

A first order approximation about the real axis across the critical strip of the continuous version of $\sqrt{\zeta(s)\zeta(1-s)}$ using a spectrally filtered linear combination of the first quiescent region truncated partial Euler Product and the simple s=1 pole.

John Martin

August 26, 2025

Executive summary

For the Riemann Zeta function $\zeta(s)$ with a pole on the real axis, a spectrally filtered linear combination of the simple pole (at $s=1$) and partial Euler Product based Riemann-Siegel formula approximation of the **normalised** Riemann Siegel Z function (such that $|Z_{norm}(s)| = |Z_{norm}(1-s)|$) can produce a useful first order approximation of 2-4 decimal place accuracy for the interval $t=(-750,750)$ about the real axis across the critical strip (without nuisance discontinuities via the fixed truncation length condition $P_{max} = 13 = 1.25 \cdot \sqrt{(\frac{750}{2\pi})^d \cdot N_C}$). Both the simple pole and the truncated partial Euler product contribute to the real axis peak behaviour and the use of fourier analysis of the **normalised** Riemann Siegel Z function approximation appears be allowing their contributions to be simply additive.

Introduction

As described in [1-3], the spectrally filtered partial Euler product approach co-opting the zeroth order Riemann-Siegel formula provided standalone useful approximations of example L-functions as $t \rightarrow \infty$. Then in [4], it was shown that the same approach can work for L-functions **without poles** around the real axis behaviour except that the truncation length should be set by the spectrum length being subject to fourier analysis in order to remove nuisance discontinuities, e.g., for the interval $t=(-750,750)$ use the fixed truncation length condition $P_{max} = 13 = 1.25 \cdot \sqrt{(\frac{750}{2\pi})^d \cdot N_C}$. However [4] also showed in the appendix that spectral filtering of the partial Euler product spectrum based on first quiescent region truncation was clearly insufficient without correction to estimate the real axis behaviour of the Riemann-Siegel Z function of the Riemann Zeta function which has a simple pole at $s=1$.

To overcome the weak performance of the spectral filtering approach near the real axis for the Riemann Zeta function two corrections to the spectrally filtered partial Euler Product approach are presented in this paper

- (i) to include the Riemann Zeta function simple pole at $s=1$ as an additional explicit term in generating the spectrum for fourier analysis,

and

- (ii) the use of fourier analysis of the normalised extended Riemann-Siegel Z function (which is the continuous version of $\sqrt{\zeta(s)\zeta(1-s)}$ and is of normalised magnitude $\left| \frac{\zeta(s)}{\sqrt{\chi(s)}} \right|$) of the Riemann Zeta function $\zeta(s)$ rather than the unnormalised extended Riemann-Siegel Z function (which is the continuous version of

$\sqrt{\zeta(s)\zeta(1-s)|\chi(s)|}$ and is of magnitude $|\zeta(s)|$ where $\chi(s)$ is the multiplicative factor in the Riemann Zeta functional equation.

$$\zeta(s) = \chi(s) \cdot \zeta(1-s) \quad (1)$$

Adding the simple pole term to the zeroth order Riemann-Siegel formula is logical given the meromorphic character of the Riemann Zeta function as encapsulated in its Euler-Maclaurin formula approximation, however it also became readily apparent in the investigation that the partial Euler Product also contributes to the magnitude of the peak in the Riemann-Siegel Z function waveform on the real axis.

In this paper, the waveform and approximation error behaviour for the sequence of progressively more complex zeroth order Riemann-Siegel formula modifications for the Riemann-Siegel Z function of the Riemann Zeta function (that are then subjected to spectral filtering and the inverse fourier transform used for estimation)

$$Z_{unnormalised,zerothRS}(s) \approx e^{-1/2 \cdot I \cdot \text{imag}(\log(\chi(s)))} \left[\prod_{p=2}^{P_{max}} \frac{1}{(1 - \frac{1}{p^s})} + \left(\prod_{p=2}^{P_{max}} \frac{1}{(1 - \frac{1}{p^{(1-s)}})} \right) \cdot \chi(s) \right] + \dots \quad A \quad (2)$$

$$Z_{norm,zerothRS}(s) \approx e^{-1/2 \cdot \log(\chi(s))} \left[\prod_{p=2}^{P_{max}} \frac{1}{(1 - \frac{1}{p^s})} + \left(\prod_{p=2}^{P_{max}} \frac{1}{(1 - \frac{1}{p^{(1-s)}})} \right) \cdot \chi(s) \right] + \dots \quad B \quad (3)$$

$$Z_{norm,zerothRSwithpole}(s) \approx e^{-1/2 \cdot \log(\chi(s))} \left[\left(\prod_{p=2}^{P_{max}} \frac{1}{(1 - \frac{1}{p^s})} \right) + \alpha' \cdot \frac{P_{max}^{(1-s)}}{s-1} + \left\{ \left(\prod_{p=2}^{P_{max}} \frac{1}{(1 - \frac{1}{p^{(1-s)}})} \right) - \alpha' \cdot \frac{P_{max}^s}{s} \right\} \cdot \chi(s) \right] + \dots \quad C \quad (4)$$

are presented for $s = 0.5 + I \cdot t$ and $s = 0.9 + I \cdot t$ in the interval $t=(-40,40)$ for the waveform and $t=(-750,750)$ for the approximation error using fourier analysis, spectral filtering, splicing and inverse fourier transformation of A, B and C based on a fourier grid spanning $t=(-750,750)$ consisting of n~150,000 points with spacing $\Delta t = 0.01$.

A basic comparison of the inverse fourier transforms of A, B and C after spectral filtering and splicing [1-4] is given in figure 1 using $P_{max} = 13$ and $\alpha' \approx 0.842$ where it can be seen that the spectral filtering of the zeroth order Riemann-Siegel formula approximation in the presence of L-function poles requires fourier analysis of the approximate **normalised** Riemann-Siegel Z function spectra which explicitly contains an appropriately scaled L-function pole contribution.

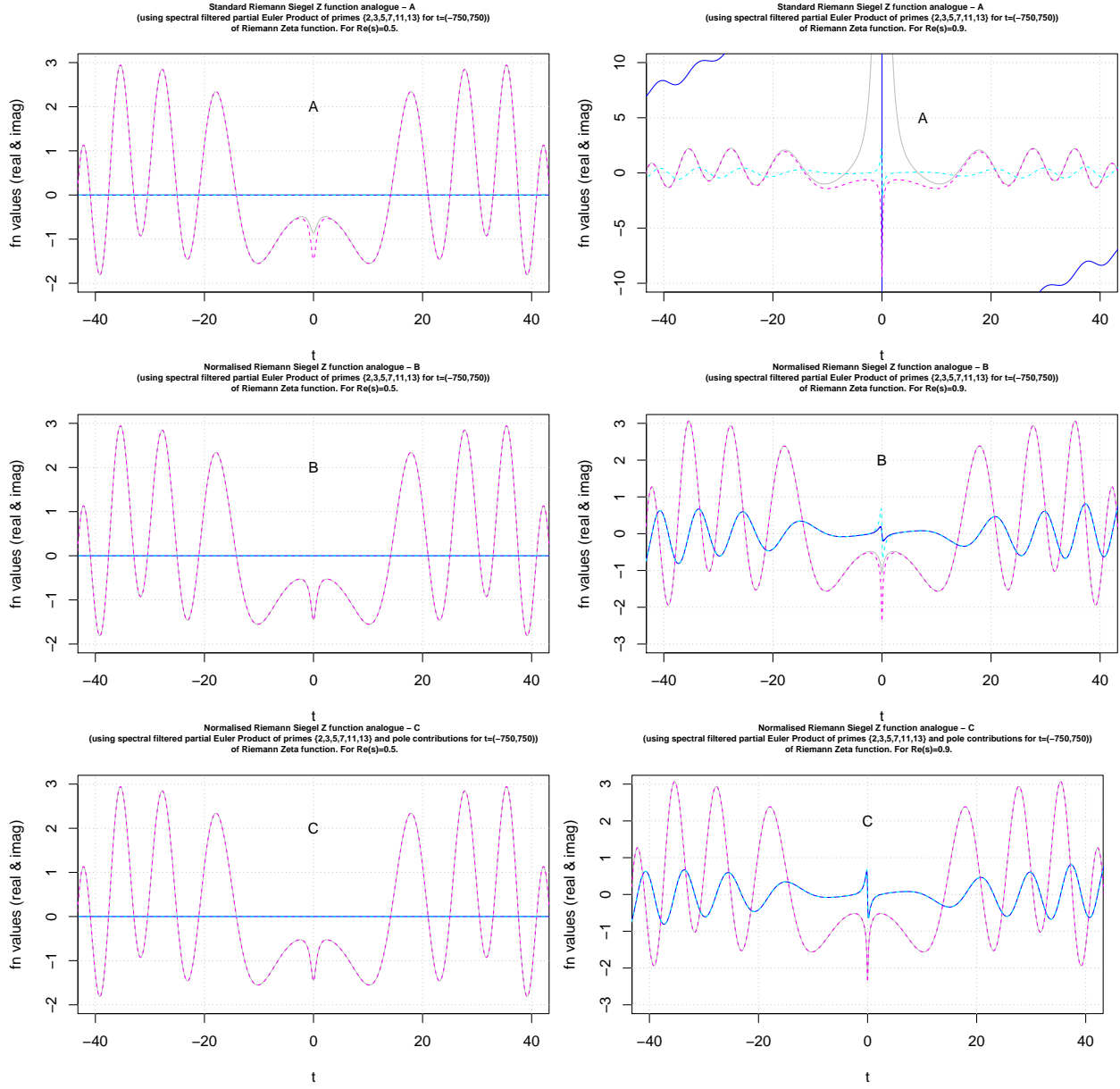


Figure 1: A comparison of the Riemann-Siegel Z function of the Riemann Zeta L-function (in standard form in row 1, in normalised form in rows 2 and 3) and three versions of spectrally filtered partial Euler Product data using truncation at $P=13$ for the interval $t=(-750,750)$ where rows 1-3 respectively display the modified zeroth order Riemann-Siegel approximations A, B and C. Both of the (true) standard and normalised Riemann-Siegel Z functions are shown in magenta (cyan) for real (imaginary) parts and the spectral filtered based EP approximation are shown in gray (blue) for real (imaginary) parts, Left column - $\sigma = 0.5$ Right column - $\sigma = 0.9$. Following the sequence A-C, figure 1 provides evidence that the partial Euler product based approximation function around $t=0$ requires both partial Euler product and pole contributions which formula C provides. The Riemann Siegel Z function and the normalised Riemann-Siegel Z function are equivalent on the critical line as $|\chi(0.5 + I \cdot t)| = 1$ (see left column). In this figure, $\alpha' = 0.842$ was the multiplicative factor used for the $s=1$ pole term in the modified zeroth order Riemann-Siegel approximation formula C.

A range of P_{max} values were investigated in this paper using $P_{max} = \max(P_{min}, 1.25 \cdot \sqrt{(\frac{750}{2\pi})})$ where $P_{min} = \{0, 2, 3, 5, 13, 238, 1009\}$ and $\prod_{p=2}^{P_{max}=0} \frac{1}{(1-1/p^s)} \equiv 1$.

In addition a range of α' constant values were investigated using $\alpha' = \{0.1, 0.8, 0.842, 0.9, 0.99\}$ to establish numerically the leading magnitude of the pole term in C.

The approximation errors are calculated respectively as

$$\text{approximation error}_A = Z_A^{\text{after spectral filtering}}(s) - e^{-1/2 \cdot I \cdot \text{imag}(\log(\chi(s)))} \zeta(s) \quad (5)$$

$$\text{approximation error}_B = Z_B^{\text{after spectral filtering}}(s) - e^{-1/2 \cdot \log(\chi(s))} \zeta(s) \quad (6)$$

$$\text{approximation error}_C = Z_C^{\text{after spectral filtering}}(s) - e^{-1/2 \cdot \log(\chi(s))} \zeta(s) \quad (7)$$

In this paper the averaging step in the fourier analysis described in [1-3] is not performed as the non-trivial zeroes are well spaced near the real axis for the Riemann Zeta function and the corresponding measured approximation errors of the final algorithm are sufficiently small for zeroth order Riemann-Siegel formula approximations B and C in the central interval of the fourier analysis.

L-functions, their unnormalised and normalised Riemann-Siegel Z function analogue versions and the zeroth order Riemann-Siegel formula definition

Of interest to this paper [5-8], the functional equation for a given L-function (and its dual L-function \bar{L})

$$L(\chi_d, s) = \chi(s) \bar{L}(\chi_d, 2k - s) \quad (8)$$

where (i) $\chi(s)$ is the complex multiplicative factor of the functional equation of the L function which can be derived from the completed L-function functional equation $\Lambda(s) = \epsilon \bar{\Lambda}(2k - s)$, (ii) χ_d are the Dirichlet characters of the corresponding Dirichlet Series and (iii) k is the critical line of the L-function defined by its complex plane symmetry behaviour.

Unnormalized Riemann-Siegel Z function

The extended unnormalised Riemann-Siegel Z function analogue of the L-function across the complex plane $s = \sigma + I \cdot t$

$$Z_{extL}(\chi_d, s) = e^{I \cdot \theta_{normextL}(s)} L(\chi_d, k - s) \quad \text{continuous function} \quad (9)$$

$$= \sqrt{|L(\chi_d, s)L(\chi_d, k - s)|} |\chi(s)| \quad \text{discontinuous version} \quad (10)$$

where the (normalised) extended Riemann-Siegel Theta function $\theta_{normextL}(t)$ is obtained from the definitions

$$\frac{\chi(s)}{|\chi(s)|} \equiv e^{-I \cdot 2\theta_{normextL}(s)} \quad (11)$$

$$\therefore \theta_{normextL}(s) = -\frac{1}{2} \cdot \text{imag} [\log (\chi(s))] \quad (12)$$

where by using only the imaginary part of the logarithm in equation (5) $\therefore |\theta_{normextL}(s)| = 1$ regardless of real(s), and hence

$$|Z_{extL}(\chi_d, s)| \equiv |L(\chi_d, s)| \quad (13)$$

is maintained in equation (2).

The **zeroth order** Riemann-Siegel formula approximation [9,10] symmetrically truncated at the first quiescent region $N_1 = \sqrt{(\frac{|t|}{2\pi})^d \cdot N_C}$ and extended across the complex plane using $\theta_{normextL}(s)$ is of the form

$$e^{I \cdot \theta_{extL}(s)} L(s) \approx e^{I \cdot \theta_{extL}(s)} \left[\sum_{n=1}^{\lfloor (\sqrt{(\frac{|t|}{2\pi})^d \cdot N_C}) \rfloor} \frac{\chi_d(n)}{n^{(s)}} + \chi(s) \cdot \sum_{n=1}^{\lfloor (\sqrt{(\frac{|t|}{2\pi})^d \cdot N_C}) \rfloor} \frac{\bar{\chi}_d(n)}{n^{(k-s)}} \right] + \dots \quad \text{as } t \rightarrow \infty \quad (14)$$

where (i) d is the degree of the L-function and (ii) N_C is the conductor of the L-function.

Normalized Riemann-Siegel Z function

The extended normalised Riemann-Siegel Z function analogue of the L-function across the complex plane $s = \sigma + I \cdot t$

$$Z_{normextL}(\chi_d, s) = e^{-\frac{1}{2} \log(\chi(s))} L(\chi_d, k - s) \quad \text{continuous function} \quad (15)$$

$$= \frac{\sqrt{L(\chi_d, s)L(\chi_d, k - s)|\chi(s)|}}{\sqrt{|\chi(s)|}} = \sqrt{L(\chi_d, s)L(\chi_d, k - s)} \quad \text{discontinuous version} \quad (16)$$

where the normalised extended Riemann-Siegel Z function is obtained from the re-arrangement of the functional equation

$$L(\chi_d, s) = \chi(s) \bar{L}(\chi_d, 2k - s) \quad (17)$$

$$\therefore \frac{L(\chi_d, s)}{\chi(s)^{\frac{1}{2}}} = \chi(s)^{\frac{1}{2}} \bar{L}(\chi_d, 2k - s) \quad \text{LHS leads to eqn (16) given eqn (10)} \quad (18)$$

$$\chi(s)^{\frac{-1}{2}} \cdot L(\chi_d, s) = \chi(s)^{\frac{1}{2}} \bar{L}(\chi_d, 2k - s) \quad (19)$$

$$e^{\frac{-1}{2} \log \chi(s)} \cdot L(\chi_d, s) = e^{\frac{1}{2} \log \chi(s)} \bar{L}(\chi_d, 2k - s) \quad \text{LHS is eqn (15)} \quad (20)$$

The normalised **zeroth order** Riemann-Siegel formula approximation then straightforwardly follows from equation (15) since only the common multiplicative factor is changed

$$e^{\frac{-1}{2} \log \chi(s)} L(s) \approx e^{\frac{-1}{2} \log \chi(s)} \left[\sum_{n=1}^{\lfloor (\sqrt{(\frac{|t|}{2\pi})^d \cdot N_C}) \rfloor} \frac{\chi_d(n)}{n^{(s)}} + \chi(s) \cdot \sum_{n=1}^{\lfloor (\sqrt{(\frac{|t|}{2\pi})^d \cdot N_C}) \rfloor} \frac{\bar{\chi}_d(n)}{n^{(k-s)}} \right] + \dots \quad \text{as } t \rightarrow \infty \quad (21)$$

where (i) d is the degree of the L-function and (ii) N_C is the conductor of the L-function.

A fourier analysis procedure for cleaning zeroth order Riemann-Siegel formula based partial Euler product based calculations of the Riemann-Siegel Z function analogue including off the critical line and simple poles of multiplicity m

Three progressively more complex modifications of the zeroth order Riemann-Siegel formula for use with spectrally filtering of partial Euler Products are presented below followed by a procedure describing the required spectral filtering, splicing, inverse fourier transformation and (optional) averaging of fourier analysis of different sample lengths to achieve improved approximation performance.

A - Modification of the zeroth order Riemann-Siegel formula for the **unnormalised** Riemann-Siegel Z function whereby the partial Euler Product is substituted for the partial Dirichlet series sum

For L-functions across the complex plane $s = \sigma + I \cdot t$. As used in [1-4], the direct partial Euler Product analogues of the first and second terms in equation (14) are

$$EP_{RS1,extL}(s, \beta) \approx e^{I \cdot \theta_{extL}(s)} \left[\prod_{p=2}^{P \leq \lfloor \beta \cdot \sqrt{(\frac{|t|}{2\pi})^d \cdot N_C} \rfloor} F_{p,L}(p^{-(s)})^{-1} \right] + \dots \quad (22)$$

$$EP_{RS2,extL}(s, \beta) \approx e^{I \cdot \theta_{extL}(s)} \cdot \chi(s) \cdot \left[\prod_{p=2}^{P \leq \lfloor \beta \cdot \sqrt{(\frac{|t|}{2\pi})^d \cdot N_C} \rfloor} F_{p,L}(p^{-(k-s)})^{-1} \right] + \dots \quad (23)$$

Therefore, the partial Euler product analogue of equation (14) is

$$Z_{L,unnormalised,zerothRS}(s, \beta) \approx EP_{RS1,extL}(s, \beta) + EP_{RS2,extL}(s, \beta) \quad (24)$$

$$\equiv Z_A(s) \quad \text{after spectral filtering} \quad (25)$$

where (i) $F_{p,L}(p^{-(s)})^{-1}$ are the Euler factors of the L-function, (ii) $\beta \geq 1$ is a hyperparameter multiplicative factor included to adjust the primes included in the Euler product(s) for the purpose of reducing the effects of spectral leakage when used in conjunction fourier analysis of these partial Euler product(s), in this paper, $\beta = 1.25$ will be used.

B - Modification of the zeroth order Riemann-Siegel formula for the **normalised** Riemann-Siegel Z function whereby the partial Euler Product is substituted for the partial Dirichlet series sum

Likewise, the direct partial Euler Product analogues of the first and second terms in equation (21) are

$$EP_{RS1,normextL}(s, \beta) \approx e^{\frac{-1}{2} \log \chi(s)} \left[\prod_{p=2}^{P \leq \lfloor \beta \cdot \sqrt{(\frac{|t|}{2\pi})^d \cdot N_C} \rfloor} F_{p,L}(p^{-(s)})^{-1} \right] + \dots \quad (26)$$

$$EP_{RS2,normextL}(s, \beta) \approx e^{\frac{-1}{2} \log \chi(s)} \cdot \chi(s) \cdot \left[\prod_{p=2}^{P \leq \lfloor \beta \cdot \sqrt{(\frac{|t|}{2\pi})^d \cdot N_C} \rfloor} F_{p,L}(p^{-(k-s)})^{-1} \right] + \dots \quad (27)$$

Therefore, the partial Euler product analogue of equation (21) is

$$Z_{L,normalised,zerothRS}(s, \beta) \approx EP_{RS1,normextL}(s, \beta) + EP_{RS2,normextL}(s, \beta) \quad (28)$$

$$\equiv Z_B(s) \quad \text{after spectral filtering} \quad (29)$$

C - Modification of the zeroth order Riemann-Siegel formula for the **normalised** Riemann-Siegel Z function whereby the partial Euler Product is substituted for the partial Dirichlet series sum **AND** explicit terms are added for the known poles of the L-function

$$EP_{RS1,normextLwithpoles}(s, \beta) \approx e^{\frac{-1}{2} \log \chi(s)} \left[\prod_{p=2}^{P \leq \lfloor \beta \cdot \sqrt{(\frac{|t|}{2\pi})^d \cdot N_C} \rfloor} F_{p,L}(p^{-(s)})^{-1} + \sum_{poles} \alpha'(pole_i, s) \frac{P_{max}^{(k-s)}}{(s - pole_i)^m} \right] + \dots \quad (30)$$

$$EP_{RS2,normextLwithpoles}(s, \beta) \approx e^{\frac{-1}{2} \log \chi(s)} \cdot \chi(s) \cdot \left[\prod_{p=2}^{P \leq \lfloor \beta \cdot \sqrt{(\frac{|t|}{2\pi})^d \cdot N_C} \rfloor} F_{p,L}(p^{-(k-s)})^{-1} + \sum_{poles} \alpha'(pole_i, k-s) \frac{P_{max}^s}{(k-s - pole_i)^m} \right] + \dots \quad (31)$$

Therefore, a partial Euler Product based analogue of the zeroth order Riemann-Siegel formula for the normalised Riemann-Siegel Z function including the presence of poles in a L-function is given by

$$Z_{L,normalised,zerothRS}(s, \beta) \approx EP_{RS1,normextLwithpoles}(s, \beta) + EP_{RS2,normextLwithpoles}(s, \beta) \quad (32)$$

$$\equiv Z_C(s) \quad \text{after spectral filtering} \quad (33)$$

where (i) $pole_i$ are the co-ordinates of simple poles for a meromorphic L-function, (ii) m is the multiplicity of the simple pole, (iii) the terms $P_{max}^{(k-s)}$ P_{max}^s appearing in equations (30) and (31) borrow the form of the second term on the RHS of the Euler-Maclaurin expansion for $\zeta(s)$ (see equation (36) below) and (iv) alpha is the linear combination coefficient for $pole_i$ required to achieve first order approximation accuracy (i.e., the approximation error is desired to be $O((\frac{1}{(k-s-pole_i)^m})^2)$ on the real line containing $pole_i$).

Partial Euler Product based zeroth order Riemann-Siegel formula fourier analysis procedure across the critical plane

For the case of a L-function using both $EP_{RS1,extL}(s, \beta)$ and $EP_{RS2,extL}(s, \beta)$ OR $EP_{RS1,normextL}(s, \beta)$ and $EP_{RS2,normextL}(s, \beta)$ calculations

1. Obtain a maximum discrete spectrum sample $\Delta t = (t_0 - 750, t_0 + 750)$, spacing 0.01, $n \sim 150,000$ for both $EP_{RS1,extL}(s, 1.25)$ and $EP_{RS2,extL}(s, 1.25)$. Using truncation at $1.25 \cdot N_1$ rather than N_1 to reduce spectral leakage from unwanted higher frequency components [1-3].
2. use spectral filtering to retain only the discrete fourier transform components of (i) $EP_{RS1,extL}(s, \beta)$ arising from primes $2, \dots, \lfloor N_1 \rfloor$ i.e., the $[0, +]$ angular frequencies and (ii) $EP_{RS2,extL}(s, \beta)$ arising from primes $2, \dots, \lfloor N_1 \rfloor$ i.e., the $(-, 0]$ angular frequencies
3. splice together the $[0, +]$ angular frequencies from $EP_{RS1,extL}(s, \beta)$ and the $(-, 0]$ angular frequencies from $EP_{RS2,extL}(s, \beta)$ using the prescription (shown in code)

```
fft_hybrid=c(1/2*(fft_plusZ[1]+fft_minusZ[1]),(fft_plusZ)[2:(ceiling(n/2)+0)],  
1/2*(fft_plusZ[ceiling(n/2)+1]+fft_minusZ[ceiling(n/2)+1]),fft_minusZ[(ceiling(n/2)+2):n])
```

where

fft_plusZ

is the discrete fourier transform of $EP_{RS1,extL}(s, \beta)$,

`fft_minusZ`

is the discrete fourier transform of $EP_{RS2,extL}(s, \beta)$, n is the discrete fourier sample length. The term
 $\{1/2*(fft_plusZ[1]+fft_minusZ[1])\}$

averages the DC component of the two zeroth order Riemann-Siegel components (giving zero imaginary component on the critical line) and the term

$\{1/2*(fft_plusZ[ceiling(n/2)+1]+fft_minusZ[ceiling(n/2)+1])\}$

averages the midway component of the n vector [3] to improve continuity of the splicing.

4. **for close spacings between non-trivial zeroes** execute and average fourier analyses of differing lengths from the original stored spectrum (e.g., averaging 100+ fourier analyses using $n \sim 127, 500 \Delta t = (t_0 - 637.5, t_0 + 637.5)$ to $n \sim 150,000 \Delta t = (t_0 - 750, t_0 + 750)$) [2,3]. The averaging prescribed this step is not performed in this paper as the non-trivial zeroes are widely spaced compared to the fourier sample grid in the examined intervals. In this paper only a single inverse fourier transform $n \sim 150000$ is returned for each example.
5. use interpolation of the final fitted results (spacing 0.01) onto a fine interpolation grid (spacing 0.00001) to estimate non-trivial zero positions. This step is not used in this paper as the non-trivial zeroes are widely spaced compared to the fourier sample grid in the examined intervals.

On the critical line $k + I \cdot t$, the simpler spectral filtering and splicing algorithm described in [3] is employed as only one component $EP_{RS1,extL}(k + I \cdot t, \beta)$ or $EP_{RS2,extL}(k + I \cdot t, \beta)$ is then needed and conjugate symmetry reflection imputation is employed to complete the improved fourier transform approximation. As noted in [3], the advantage of using the Riemann-Siegel Z function analogue for fourier analysis is that the above splicing specification only involves n the sample length.

The input discrete spectra samples are calculated using Pari-GP [11] and the fourier transforms, inverse fourier transforms, spectral filtering and graphing is performed using R [12] and RStudio IDE [13]. The Rmd version of this paper contains the r script used in producing the fourier analysis and graphs.

The Riemann Zeta L-function

The first degree L function, Riemann Zeta L function 1-1-1.1-r0-0-0 [8] under the arithmetic version of the L-function is written in dirichlet series form as

$$\zeta(s) = \sum_{k=1}^{\infty} \left(\frac{1}{k^s} \right) \quad (34)$$

The above infinite dirichlet series is only convergent for $\Re(s) > 1$ with its known non-trivial zeroes (so far) lying on the critical line $s = 0.5 + I \cdot t$

The Riemann Zeta function is defined [5-7], in the complex plane by the integral

$$\zeta(s) = \frac{\prod(-s)}{2\pi i} \int_{C_{\epsilon,\delta}} \frac{(-x)^s}{(e^x - 1)x} dx \quad (35)$$

where $s \in \mathbb{C}$ and $C_{\epsilon,\delta}$ is the contour about the imaginary poles. The Riemann Zeta function Euler-Maclaurin approximation [5-7] is given by

$$\zeta(s) \approx \sum_{k=1}^{(n-1)} \left(\frac{1}{k^s} \right) + \frac{n^{(1-s)}}{s-1} + \frac{1}{2n^s} + \sum_{i=1} \frac{B_{2i}}{(2i)!} \frac{(s+2i-2)!}{(s-1)!n^{(s+2i-1)}} \quad (36)$$

The Riemann Zeta function has been shown to obey the functional equation [5-8]

$$\zeta(s) = \chi_\zeta(s)\zeta(1-s) \quad (37)$$

$$= 2^s \pi^{s-1} \sin\left(\frac{\pi s}{2}\right) \Gamma(1-s) \zeta(1-s) \quad (38)$$

The Riemann Zeta L-function is a degree 1 L-function ($d=1$) and its conductor value is 1 [8]. Hence the first quiescent region of the dirichlet series of $\zeta(s)$ is given by

$$N_1 = \left\lfloor \sqrt{\left(\frac{t}{2\pi}\right)^1 \cdot 1} \right\rfloor = \left\lfloor \sqrt{\frac{t}{2\pi}} \right\rfloor \quad (39)$$

The two functions of interest to be approximated by partial Euler Products for fourier analysis and spectral filtering are the

unnormalised extended Riemann-Siegel Z function of $\zeta(s)$

$$Z_{ext\zeta}(s) = e^{-1/2 \cdot I \cdot imag[\log(\chi_\zeta(s))]} \zeta(s) \quad (40)$$

$$= e^{I\theta_{ext\zeta}(s)} \zeta(s) \quad (\text{continuous version}) \quad (41)$$

$$= \sqrt{\zeta(s)\zeta(1-s)|\chi_\zeta(s)|} \quad (\text{discontinuous version}) \quad (42)$$

and the

normalised extended Riemann-Siegel Z functions of $\zeta(s)$

$$Z_{normext\zeta}(s) = e^{-1/2 \cdot \log(\chi_\zeta(s))} \zeta(s) \quad (\text{continuous version}) \quad (43)$$

$$= \sqrt{\zeta(s)\zeta(1-s)} \quad (\text{discontinuous version}) \quad (44)$$

across the complex plane.

Therefore using the above Riemann Zeta L-function information the following three partial Euler product based modifications of the zeroth order Riemann-Siegel formula for the Riemann Zeta function are presented in this paper.

A - Modification of the zeroth order Riemann-Siegel formula for the **unnormalised** Riemann-Siegel Z function of the Riemann Zeta L-function whereby the partial Euler Product is substituted for the partial Dirichlet series sum

$$Z_{\zeta, unnormalised, zerothRS}(s) \approx e^{-1/2 \cdot I \cdot imag(\log(\chi(s)))} \left[\prod_{p=2}^{P_{max}} \frac{1}{(1 - \frac{1}{p^s})} + \left(\prod_{p=2}^{P_{max}} \frac{1}{(1 - \frac{1}{p^{(1-s)}})} \right) \cdot \chi(s) \right] + \dots = Z_A \quad (45)$$

B - Modification of the zeroth order Riemann-Siegel formula for the **normalised** Riemann-Siegel Z function of the Riemann Zeta L-function whereby the partial Euler Product is substituted for the partial Dirichlet series sum

$$Z_{\zeta, \text{norm}, \text{zerothRS}}(s) \approx e^{-1/2 \cdot \log(\chi(s))} \left[\prod_{p=2}^{P_{max}} \frac{1}{(1 - \frac{1}{p^s})} + \left(\prod_{p=2}^{P_{max}} \frac{1}{(1 - \frac{1}{p^{(1-s)}})} \right) \cdot \chi(s) \right] + \dots = Z_B \quad (46)$$

C - Modification of the zeroth order Riemann-Siegel formula for the **normalised** Riemann-Siegel Z function of the Riemann Zeta L-function whereby the partial Euler Product is substituted for the partial Dirichlet series sum **AND** explicit terms are added for the known pole at s=1 of $\zeta(s)$

$$Z_{\zeta, \text{norm}, \text{zerothRSwithpole}}(s) \approx e^{-1/2 \cdot \log(\chi(s))} \left[\left(\prod_{p=2}^{P_{max}} \frac{1}{(1 - \frac{1}{p^s})} \right) + \alpha' \cdot \frac{P_{max}^{(1-s)}}{s-1} + \left\{ \left(\prod_{p=2}^{P_{max}} \frac{1}{(1 - \frac{1}{p^{(1-s)}})} \right) - \alpha' \cdot \frac{P_{max}^s}{s} \right\} \cdot \chi(s) \right] + \dots = Z_C \quad (47)$$

where in equation (47) ideally a good choice of α' should result in the approximation error being $O(\left(\frac{1}{(s-1)}\right)^2)$ in the region of the pole.

As stated in the introduction the approximation errors of the equations (45-47) after spectral filtering are calculated via

$$\text{approximation error}_A = Z_A^{\text{after spectral filtering}}(s) - e^{-1/2 \cdot I \cdot \text{imag}(\log(\chi(s)))} \zeta(s) \quad (48)$$

$$\text{approximation error}_B = Z_B^{\text{after spectral filtering}}(s) - e^{-1/2 \cdot \log(\chi(s))} \zeta(s) \quad (49)$$

$$\text{approximation error}_C = Z_C^{\text{after spectral filtering}}(s) - e^{-1/2 \cdot \log(\chi(s))} \zeta(s) \quad (50)$$

In this paper, to investigate the impact of the the truncation length P_{max} , $P_{max} \leq \max(P_{min}, (\lfloor \beta \cdot \sqrt{(\frac{|t|}{2\pi})^d \cdot N_C} \rfloor))$ replaces $P_{max} \leq \lfloor \beta \cdot \sqrt{(\frac{|t|}{2\pi})^d \cdot N_C} \rfloor$ from equations (22,23,26,27,30,31)

As identified in this investigation only the normalised Riemann-Siegel Z function approximation C (after spectral filtering), equations (3,48) straightforwardly allows $O(\left(\frac{1}{(s-1)}\right)^2)$ approximation error for the Riemann-Siegel Z function of the Riemann Zeta L-function within the critical strip around the real axis.

Results

Z_A, Z_B, Z_C behaviour for P=13, $\alpha' \sim 0.842$

Figure 1 illustrates in the performance of the averaged inverse fourier transform around the real axis compared to the real (imaginary) parts of the true Riemann-Siegel Z function shown in magenta (cyan) at the fourier grid spacing 0.01, for approximations A, B, C in rows 1-3 respectively using $P_{max} = 13$. The lefthand (righthand) panels display the $\sigma = 0.5$ ($\sigma = 0.9$) behaviour for the interval $t=(-40,40)$.

The first row behaviour was also presented in [4] and shows that approximation A (after spectral filtering) is insufficient to accurately approximate the Riemann-Siegel Z function behaviour of the Riemann Zeta function in the critical strip nearby the $s=1$ pole. Of particular concern is the glaring discrepancy in the approximation A fit for $\sigma = 0.9$ (first row, righthand panel) compared to the true function.

In contrast, the approximation B (after spectral filtering) results in the middle row of figure 1, where the approximation for $\text{imag}(Z_B)$ (shown in blue) is much closer to the true function behaviour at $t=0$.

Finally, the approximation C (after spectral filtering) which explicitly includes the $s=1$ pole in the zeroth order Riemann-Siegel formula modification can reasonably reproduce the true function behaviour with $\alpha' \sim 0.842$ which is a logical model containing both Euler product and pole contributions given the Riemann Zeta function is a meromorphic function with a pole at $s=1$.

Of some interest, is whether the above discrepancies in approximations A, B and C in figure 1 reveal themselves in the fourier analysis.

Figure 2 examines the fourier spectra of Z_A and the unnormalised Riemann-Siegel Z function given the interval $t=(-750,750)$ for $\sigma = 0.5$. The lefthand spectra in the top and bottom rows shows the fourier spectra of the two components of Z_A and the righthand panels of the same rows indicate the useful spectra after spectral filtering and mirror conjugation. In the middle row is the fourier spectra of the true unnormalised Riemann-Siegel Z function repeated twice. Comparing the top and bottom rows of the righthand panel with the middle row it is difficult to see any obvious differences with the true function.

Figure 3 examines the fourier spectra of Z_A and the unnormalised Riemann-Siegel Z function given the interval $t=(-750,750)$ for $\sigma = 0.9$. The lefthand spectra in the top and bottom rows shows the fourier spectra of the two components of Z_A and the righthand panels of the same rows indicate the useful spectra after spectral filtering. In the lefthand panel of the middle row is the fourier spectra of the true unnormalised Riemann-Siegel Z function and the righthand panel splices the useful parts of the first and second components of Z_A together. The extremely high fourier signal about the DC component in the bottom row and the -ve frequencies in the righthand panel of the middle row indicates serious accuracy issues with the second component of Z_A as the $\text{Re}(s) \rightarrow s = 1$. Another feature of interest is the extra thickness of the shoulders of the fourier spectra of the true **unnormalised** Riemann-Siegel Z function lefthand panel - middle row for $\sigma = 0.9$ which Z_A doesn't replicate.

Figure 4 examines the fourier spectra of Z_B and the normalised Riemann-Siegel Z function given the interval $t=(-750,750)$ for $\sigma = 0.5$. The lefthand spectra in the top and bottom rows shows the fourier spectra of the two components of Z_B and the righthand panels of the same rows indicate the useful spectra after spectral filtering and mirror conjugation. In the middle row is the fourier spectra of the true **normalised** Riemann-Siegel Z function repeated twice. Comparing the top and bottom rows of the righthand panel with the middle row it is difficult to see any obvious differences with the true function.

Figure 5 examines the fourier spectra of Z_B and the normalised Riemann-Siegel Z function given the interval $t=(-750,750)$ for $\sigma = 0.9$. The lefthand spectra in the top and bottom rows shows the fourier spectra of the two components of Z_B and the righthand panels of the same rows indicate the useful spectra after spectral filtering. In the lefthand panel of the middle row is the fourier spectra of the true normalised Riemann-Siegel Z function and the righthand panel splices the useful parts of the first and second components of Z_B together. Comparing lefthand and righthand panels of the middle row it is difficult to see any obvious differences with the true function. Of particular interest however, is that the extra thickness of the shoulders of the fourier spectra present in the true **unnormalised** Riemann-Siegel Z function lefthand panel - middle row for figure 3 of Z_A doesn't occur for the true **normalised** Riemann-Siegel Z function lefthand panel - middle row for figure 5 of Z_B . Therefore it can be surmised that fourier spectra of the true **normalised** Riemann-Siegel Z function doesn't contain particular frequencies present in the fourier spectra of the **unnormalised** Riemann-Siegel Z function.

Figure 6 examines the fourier spectra of Z_C and the normalised Riemann-Siegel Z function given the interval $t=(-750,750)$ for $\sigma = 0.5$. The lefthand spectra in the top and bottom rows shows the fourier spectra of the two components of Z_C and the righthand panels of the same rows indicate the useful spectra after spectral filtering and mirror conjugation. In the middle row is the fourier spectra of the true **normalised** Riemann-Siegel Z function repeated twice. Comparing the top and bottom rows of the righthand panel with the middle row it is difficult to see any obvious differences with the true function.

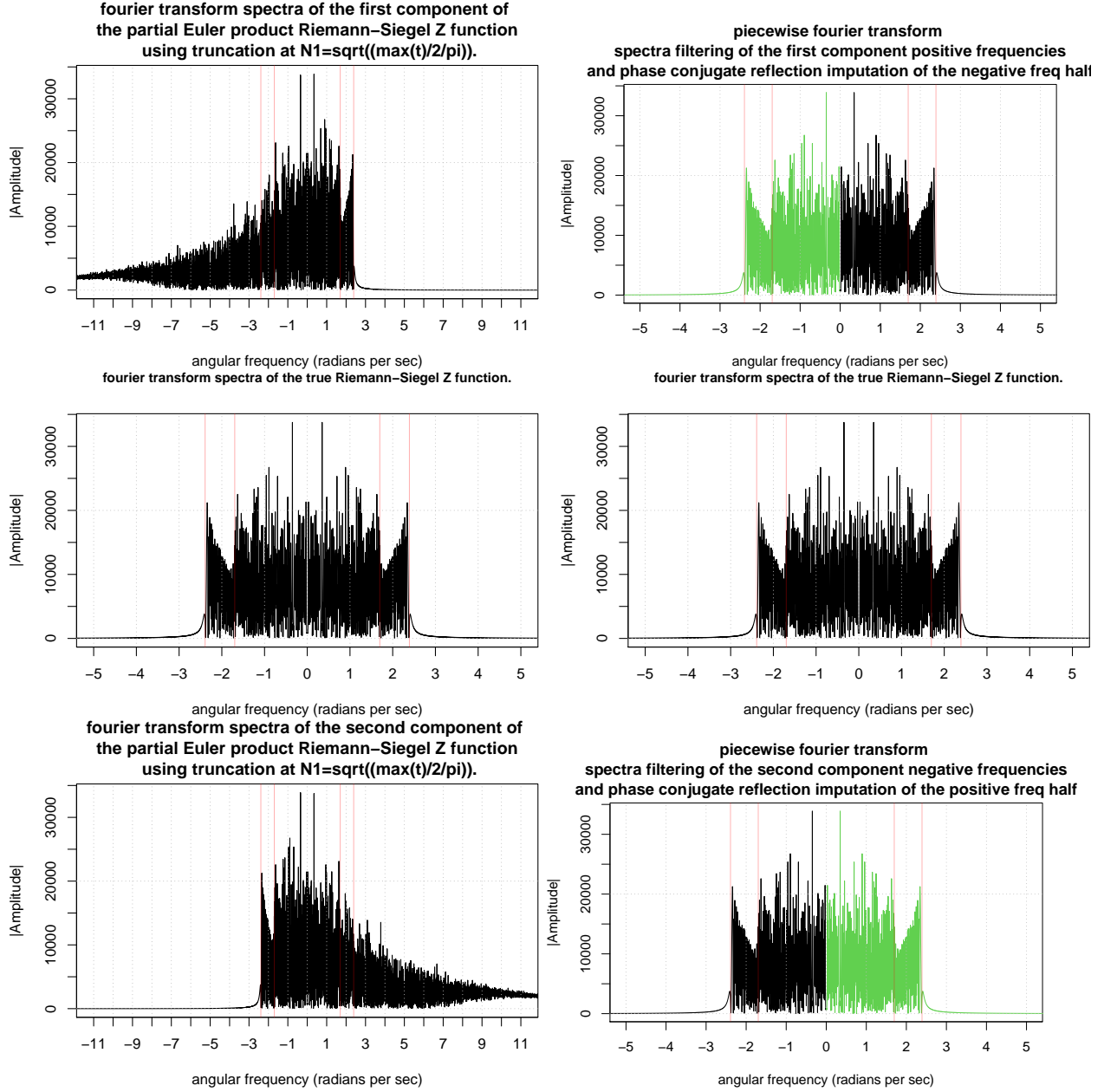


Figure 2: A comparison of the fourier transforms of the Riemann-Siegel Z function analogue of the $\zeta(s)$ L-function and partial Euler Product using truncation at $P=13$ in the complex plane at $\sigma = 1/2$ for the interval $t=(-750,750)$ about the real axis. On the critical line, to help use the partial Euler Product as an approximation of the Riemann-Siegel Z function phase conjugate reflection of the (accurate part of) partial Euler Product fourier transform about angular frequency = zero as shown in green is a strong zeroth order improvement. The middle row lefthand panel displays the true Riemann-Siegel Z function fourier transform behaviour.

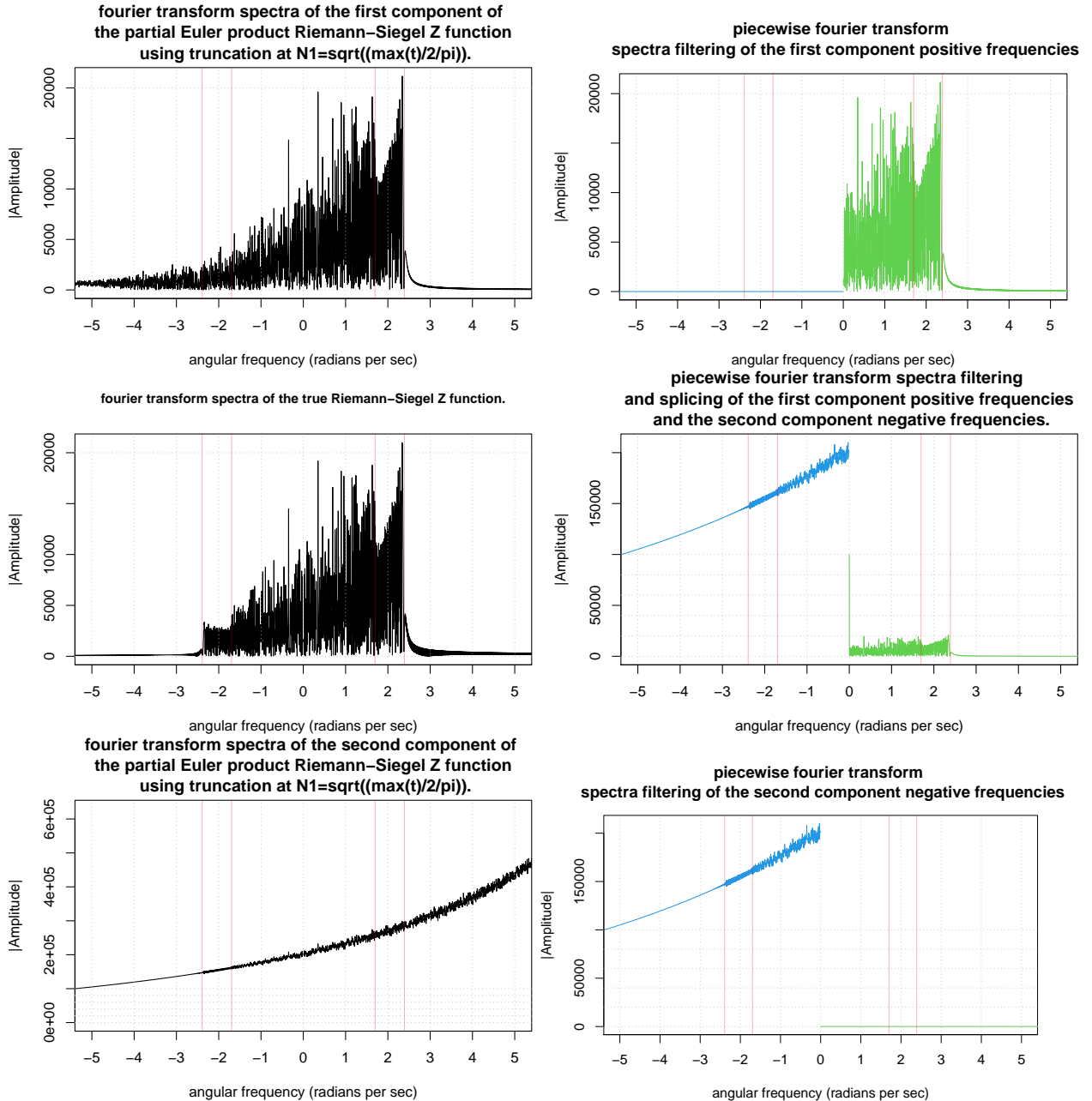


Figure 3: A comparison of the Fourier transforms of the Riemann-Siegel Z function analogue Z_A of the $\zeta(s)$ L-function and partial Euler Product using truncation at $P=13$ in the complex plane at $\sigma = 0.9$ for the interval $t=(-750,750)$ about the real axis. Off the critical line, to help use the partial Euler Product as an approximation of the Riemann-Siegel Z function only the positive frequencies (green) negative frequencies (blue) of the first and second Riemann-Siegel components are retained and spliced together. In the middle row, the **lefthand panel** displays the true Riemann-Siegel Z function Fourier transform behaviour while the **righthand panel** displays the neat splicing together of the first and second Riemann-Siegel components Fourier transform behaviour.

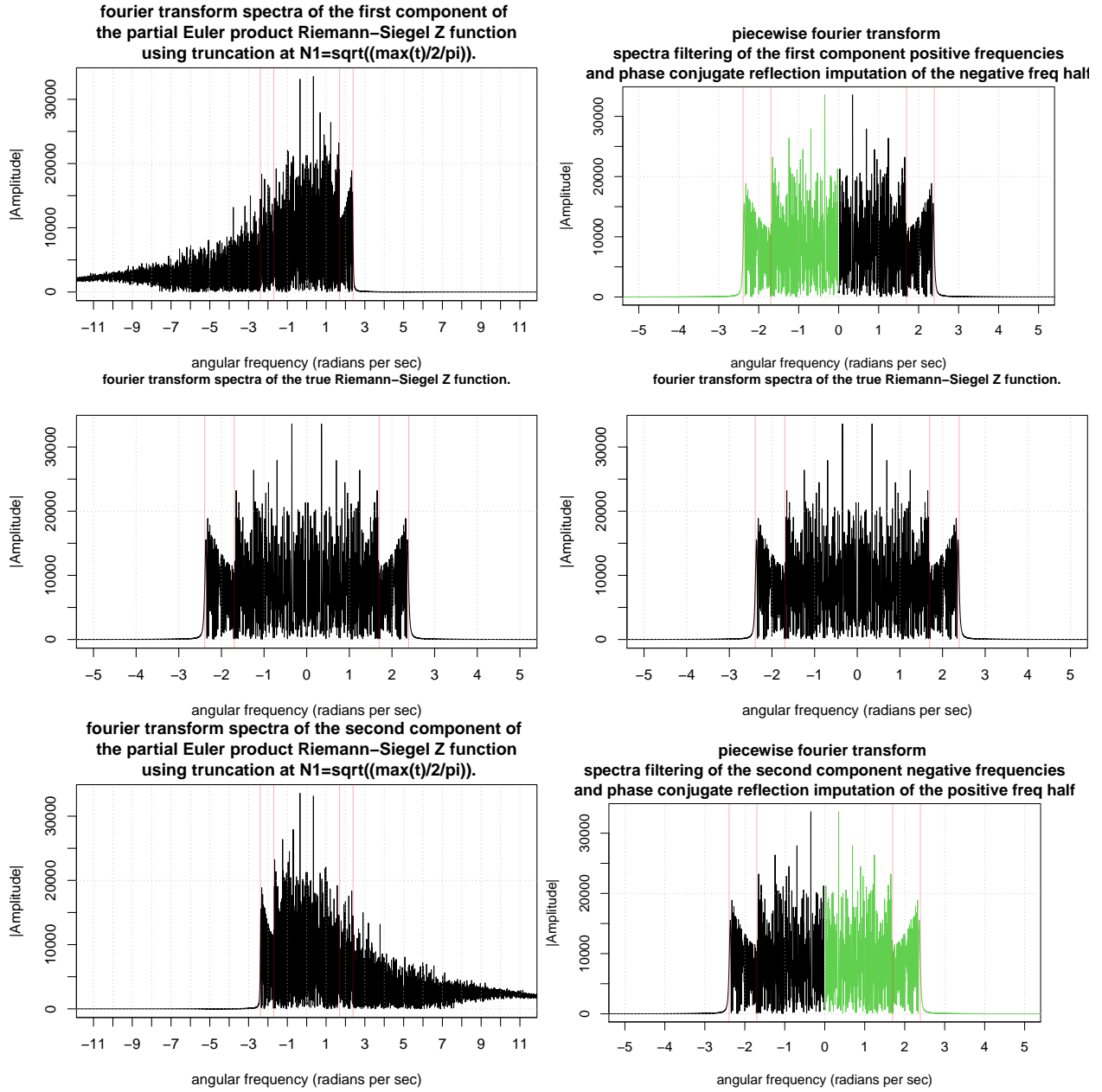
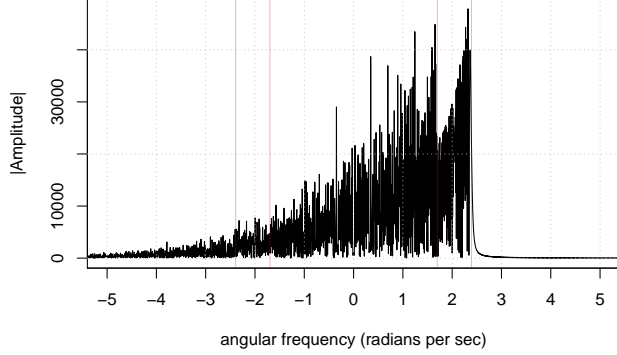
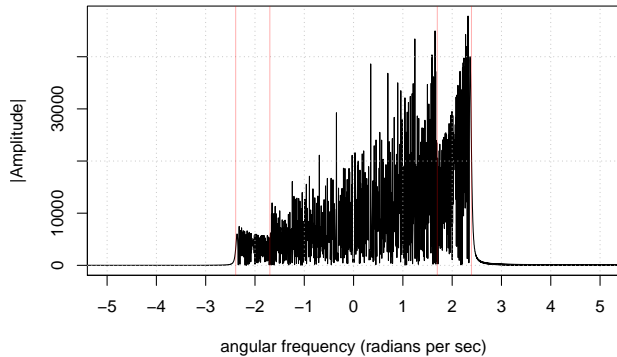


Figure 4: A comparison of the Fourier transforms of the Riemann-Siegel Z function analogue Z_B of the $\zeta(s)$ L-function and partial Euler Product using truncation at $P=13$ in the complex plane at $\sigma = 1/2$ for the interval $t=(-750,750)$ about the real axis. On the critical line, to help use the partial Euler Product as an approximation of the Riemann-Siegel Z function phase conjugate reflection of the (accurate part of) partial Euler Product Fourier transform about angular frequency = zero as shown in green is a strong zeroth order improvement. The middle row lefthand panel displays the true Riemann-Siegel Z function Fourier transform behaviour.

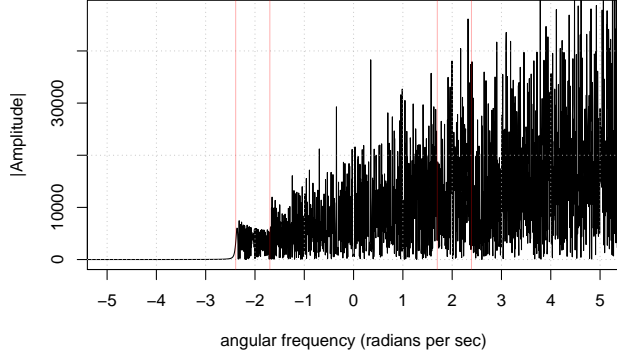
fourier transform spectra of the first component of
the partial Euler product Riemann–Siegel Z function
using truncation at $N1=\sqrt{(\max(t)/2\pi)}$.



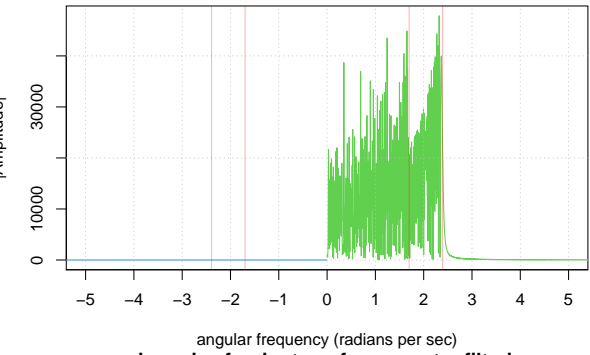
fourier transform spectra of the true Riemann–Siegel Z function.



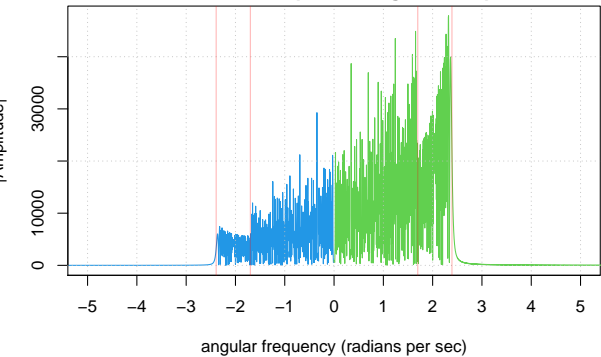
fourier transform spectra of the second component of
the partial Euler product Riemann–Siegel Z function
using truncation at $N1=\sqrt{(\max(t)/2\pi)}$.



piecewise fourier transform
spectra filtering of the first component positive frequencies



piecewise fourier transform spectra filtering
and splicing of the first component positive frequencies
and the second component negative frequencies.



piecewise fourier transform
spectra filtering of the second component negative frequencies

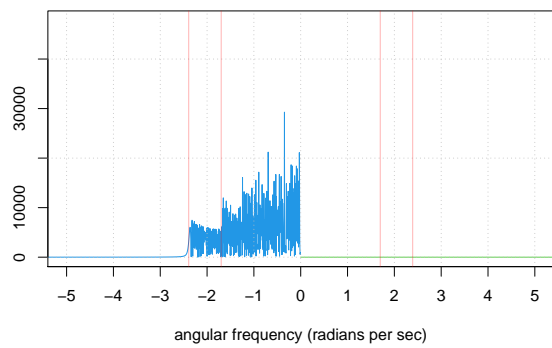


Figure 5: A comparison of the fourier transforms of the Riemann-Siegel Z function analogue Z_B of the $\zeta(s)$ L-function and partial Euler Product using truncation at $P=13$ in the complex plane at $\sigma = 0.9$ for the interval $t=(-750,750)$ about the real axis. Off the critical line, to help use the partial Euler Product as an approximation of the Riemann-Siegel Z function only the positive frequencies (green) negative frequencies (blue) of the first and second Riemann-Siegel components are retained and spliced together. In the middle row, the **lefthand panel** displays the true Riemann-Siegel Z function fourier transform behaviour while the **righthand panel** displays the neat splicing together of the first and second Riemann-Siegel components fourier transform behaviour.

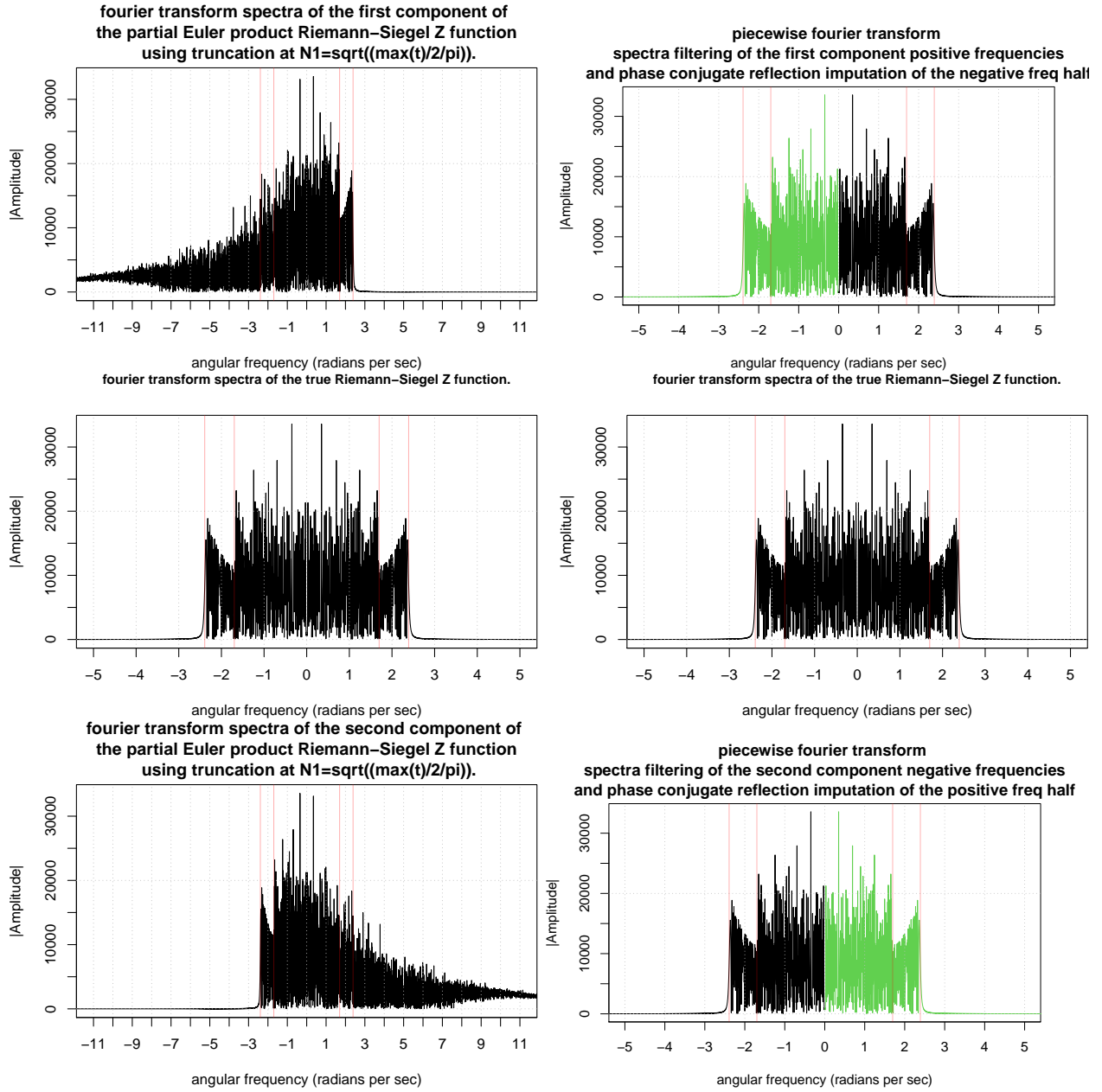
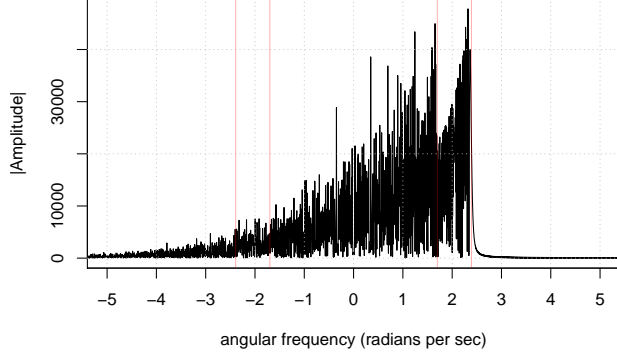
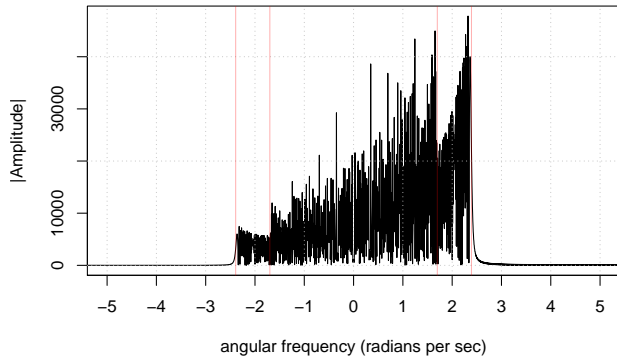


Figure 6: A comparison of the Fourier transforms of the Riemann-Siegel Z function Z_C analogue of the $\zeta(s)$ L-function and partial Euler Product using truncation at $P=13$ in the complex plane at $\sigma = 1/2$ for the interval $t=(-750,750)$ about the real axis. On the critical line, to help use the partial Euler Product as an approximation of the Riemann-Siegel Z function phase conjugate reflection of the (accurate part of) partial Euler Product Fourier transform about angular frequency = zero as shown in green is a strong zeroth order improvement. The middle row lefthand panel displays the true Riemann-Siegel Z function Fourier transform behaviour.

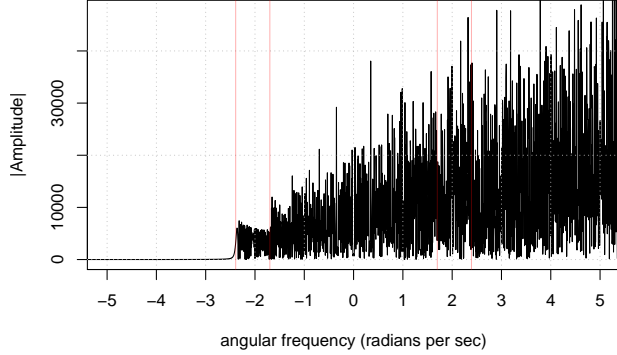
fourier transform spectra of the first component of
the partial Euler product Riemann–Siegel Z function
using truncation at $N1=\sqrt{(\max(t)/2\pi)}$.



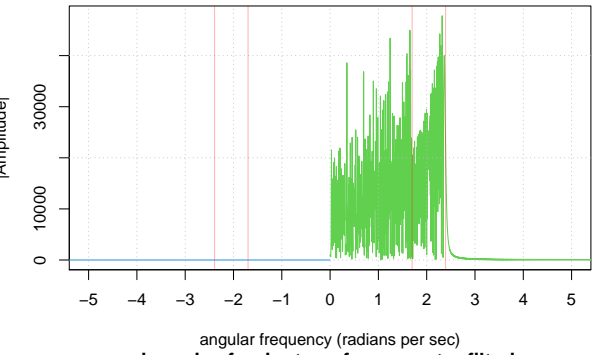
fourier transform spectra of the true Riemann–Siegel Z function.



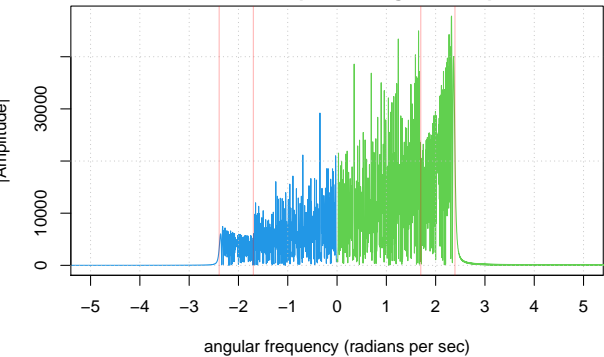
fourier transform spectra of the second component of
the partial Euler product Riemann–Siegel Z function
using truncation at $N1=\sqrt{(\max(t)/2\pi)}$.



piecewise fourier transform
spectra filtering of the first component positive frequencies



piecewise fourier transform spectra filtering
and splicing of the first component positive frequencies
and the second component negative frequencies.



piecewise fourier transform
spectra filtering of the second component negative frequencies

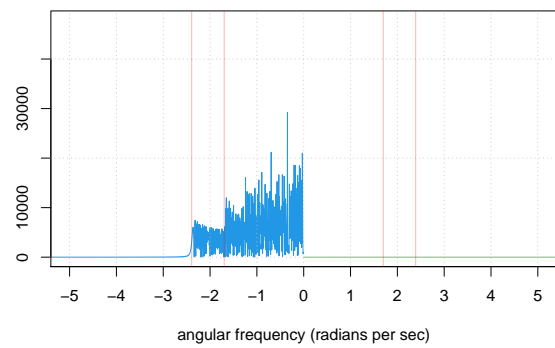


Figure 7: A comparison of the fourier transforms of the Riemann-Siegel Z function analogue Z_C of the $\zeta(s)$ L-function and partial Euler Product using truncation at $P=13$ in the complex plane at $\sigma = 0.9$ for the interval $t=(-750,750)$ about the real axis. Off the critical line, to help use the partial Euler Product as an approximation of the Riemann-Siegel Z function only the positive frequencies (green) negative frequencies (blue) of the first and second Riemann-Siegel components are retained and spliced together. In the middle row, the **lefthand panel** displays the true Riemann-Siegel Z function fourier transform behaviour while the **righthand panel** displays the neat splicing together of the first and second Riemann-Siegel components fourier transform behaviour.

Figure 7 examines the fourier spectra of Z_C and the normalised Riemann-Siegel Z function given the interval $t=(-750,750)$ for $\sigma = 0.9$. The lefthand spectra in the top and bottom rows shows the fourier spectra of the two components of Z_C and the righthand panels of the same rows indicate the useful spectra after spectral filtering. In the lefthand panel of the middle row is the fourier spectra of the true normalised Riemann-Siegel Z function and the righthand panel splices the useful parts of the first and second components of Z_B together. Comparing lefthand and righthand panels of the middle row it is difficult to see any obvious differences with the true function.

Thus comparing the fourier spectra shows differences (i) between Z_A and Z_B , Z_C and (ii) the true unnormalised and normalised functions. However, figure 1 is better at showing the differences between Z_B and Z_C .

Z_B, Z_C behaviour for various partial Euler Product truncation lengths up to P=13, $\alpha' \sim 0.842$

Given spectrally filtered Z_B and Z_C are more robust approximations to Riemann-Siegel Z function behaviour the following investigations only examine Z_B and Z_C performance.

In the lefthand panels of figure 8 the following interval $s = (0.9 - I \cdot 40, 0.9 + I \cdot 40)$ is displayed for five different values of the minimum prime in Z_B partial Euler product calculation $P_{min} = \left\lfloor \max \left(\{1, 2, 3, 5, 13\}, 1.25 \cdot \sqrt{\left(\frac{t}{2\pi}\right)^d \cdot N_C} \right) \right\rfloor$ with each row (top to bottom) respectively belonging to the minimum prime value $\{1,2,3,5,13\}$ which is active when $t=0$. When $P_{min} = 1$, the partial Euler Product returns the value unity.

In the righthand panels, the real part of the approximation error equation (49) for Z_B is displayed over the entire span of the input spectra $s = (0.9 - I \cdot 750, 0.9 + I \cdot 750)$

In the lefthand panels of figure 8 the following interval $s = (0.9 - I \cdot 40, 0.9 + I \cdot 40)$ is displayed for five different values of the minimum prime in Z_C partial Euler product calculation $P_{min} = \left\lfloor \max \left(\{1, 2, 3, 5, 13\}, 1.25 \cdot \sqrt{\left(\frac{t}{2\pi}\right)^d \cdot N_C} \right) \right\rfloor$ with each row (top to bottom) respectively belonging to the minimum prime value $\{1,2,3,5,13\}$ which is active when $t=0$. When $P_{min} = 1$, the partial Euler Product returns the value unity.

In the righthand panels, the real part of the approximation error equation (50) for Z_C is displayed over the entire span of the input spectra $s = (0.9 - I \cdot 750, 0.9 + I \cdot 750)$

It can be seen from figures 8 and 9 that for the interval $t=(-750,750)$

- (i) as the number of primes involved in the partial Euler Product approximation increases the nuisance discontinuities caused by steps through P_{min} are removed
- (ii) there is residual error in the approximations at $t=0$ with Z_C having much lower error by explicit inclusion of the pole at $s=1$ (when $\alpha' \sim 0.842$).

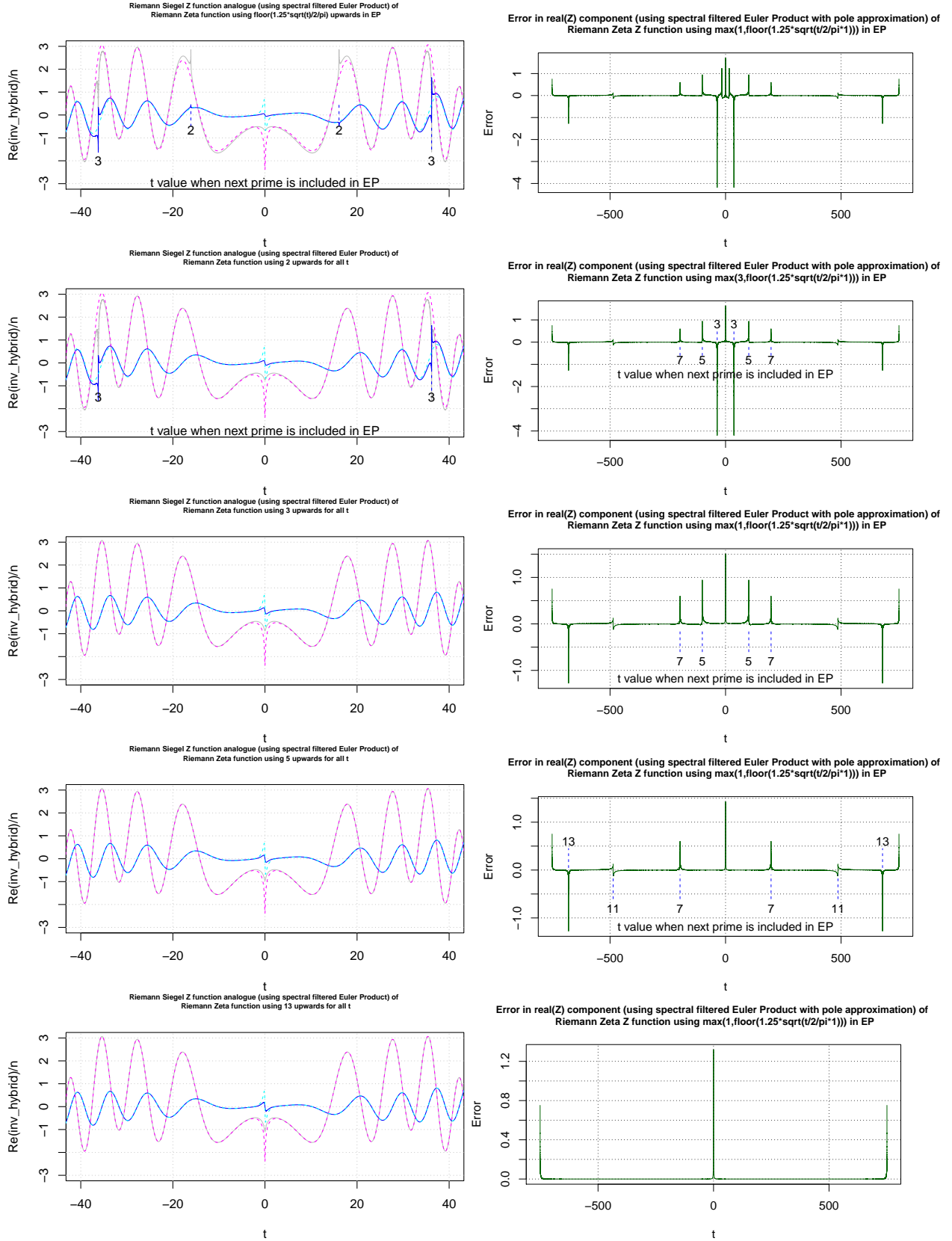


Figure 8: Lefthand panel - True Z function shown in magenta (cyan) for real (imaginary) parts and spectral filtered based EP approximation shown in gray (blue) for real (imaginary) parts, Right hand panel - Error in the real(Z) darkgreen EP approximation. A comparison of the Riemann-Siegel Z function of the Riemann Zeta L-function and spectrally filtered partial Euler Product (using truncation at $\max(P, 1.25 \cdot \sqrt{((\frac{|t|}{2\pi})^1 \cdot 1)})$) in the complex plane at $\sigma = 0.9$ for the interval $t=(-750,750)$ where $P_{\min} = 1, 2, 3, 5, 13$ for rows 1-5. The approximation error around $t=0$ does not disappear by adding primes.

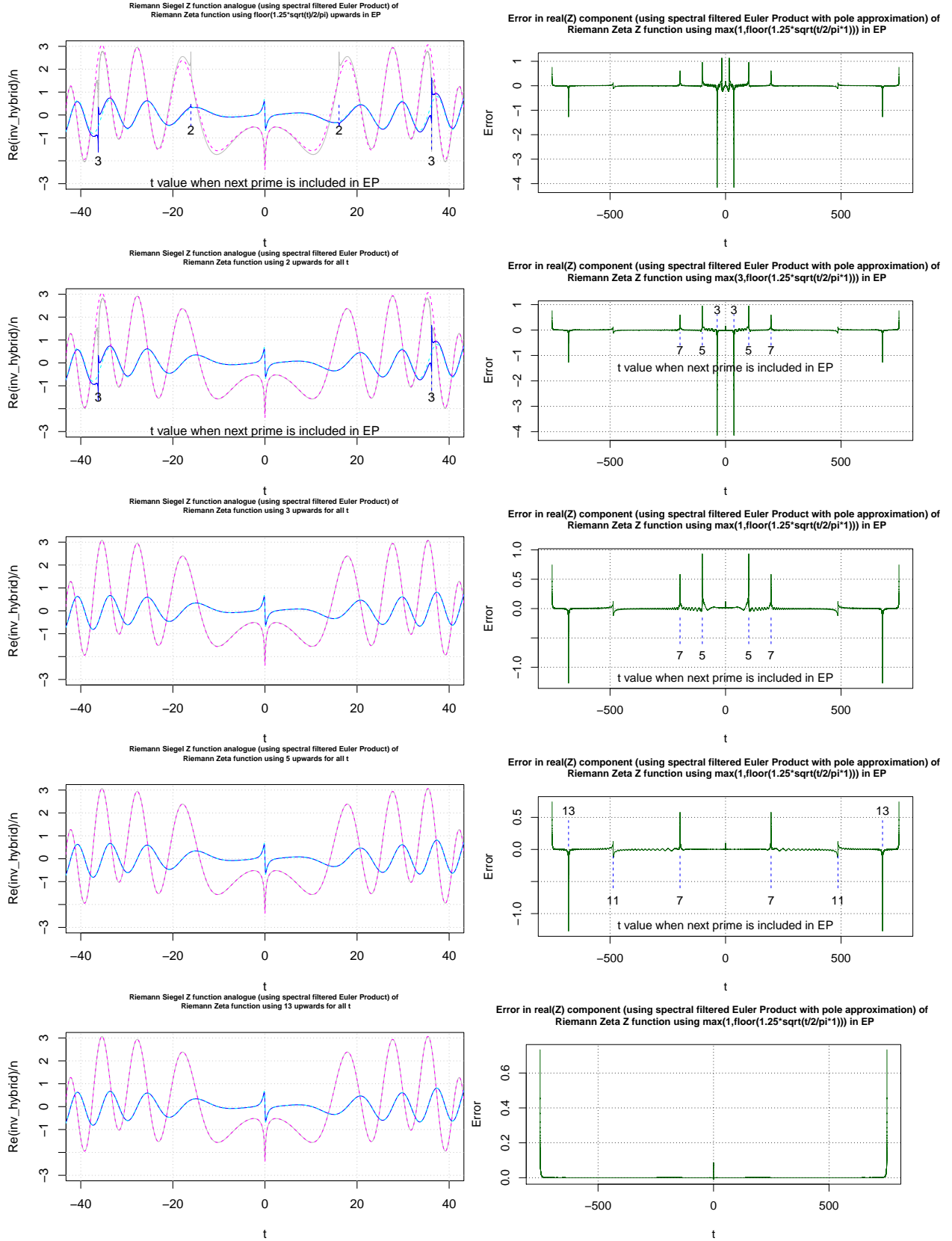


Figure 9: Lefthand panel - True Z function shown in magenta (cyan) for real (imaginary) parts and spectral filtered based EP approximation shown in gray (blue) for real (imaginary) parts, Right hand panel - Error in the real(Z) darkgreen EP approximation. A comparison of the Riemann-Siegel Z function of the Riemann Zeta L-function and spectrally filtered partial Euler Product (using truncation at $\max(P, 1.25 \cdot \sqrt{((\frac{|t|}{2\pi})^1 \cdot 1)})$) in the complex plane at $\sigma = 0.9$ for the interval $t=(-750,750)$ where $P_{min} = 1, 2, 3, 5, 13$ for rows 1-5. The approximation error around $t=0$ does not disappear by adding primes.

Z_C behaviour for $t=(-4,4)$ with in the critical strip for longer Euler Product truncation lengths, $\alpha' \sim 0.842$

In the lefthand panels of figure 10 the following interval $s = (0.5 - I \cdot 4, 0.5 + I \cdot 4)$ is displayed for five different increased values of the minimum prime in Z_C partial Euler product calculation $P_{min} = \left\lfloor \max \left(\{13, 23, 33, 238, 1009\}, 1.25 \cdot \sqrt{\left(\frac{t}{2\pi}\right)^d \cdot N_C} \right) \right\rfloor$ with each row (top to bottom) respectively belonging to the minimum prime value $\{13, 23, 33, 238, 1009\}$ which is active when $t=0$.

In the righthand panels, the real and imaginary parts of the approximation error equation (50) for Z_C is displayed over the central interval of the input spectra $s = (0.5 - I \cdot 4, 0.5 + I \cdot 4)$

It can be seen from figure 10 that for the interval $t=(-4,4)$ (using fourier analysis of $\sim 150,000$ points in the interval $t=(-750,750)$)

- (i) as the number of primes involved in the partial Euler Product approximation increases beyond 13 the approximation error firstly reduces and then eventually increases for the highest $P_{min}=1009$. The $P=238$ value displays the smallest approximation error and it is noted that $P=238$ was intentionally selected because $N_2 = \lfloor \frac{750}{\pi} \rfloor = 238$ corresponds to the second quiescent region of the Dirichlet series of $\zeta(s)$.
- (ii) the line shape of the approximation error (except for $P_{min}=1009$) is qualitatively $O\left(\left(\frac{1}{(s-1)}\right)^2\right)$ providing evidence that using $\alpha' \sim 0.842$ is achieving the intended design of Z_C . However, similar analysis for $\sigma = 0.9$ does not obtain the same value as $\alpha' \sim 0.842$
- (iii) the fourier analysis is a double precision calculation which eventually fails for large enough truncation length when $t=0$ for the Riemann Zeta Euler product. This is because the input partial Riemann Zeta function Euler Product spectra has a peak at $t=0$ which rapidly increases with truncation length.

Z_C behaviour for $t=(-4,4)$ within the critical strip for $P=13$, as a function of the linear mixture of the pole contribution i.e. using various α' values

In the lefthand panels of figure 11 the following interval $s = (0.5 - I \cdot 4, 0.5 + I \cdot 4)$ is displayed for five different increased values of the minimum prime in Z_C partial Euler product calculation $P_{min} = 13$ with each row (top to bottom) respectively belonging to the different α' values $\{0.1, 0.8, 0.842, 0.9, 0.99\}$.

In the righthand panels, the real and imaginary parts of the approximation error equation (50) for Z_C is displayed over the central interval of the input spectra $s = (0.5 - I \cdot 4, 0.5 + I \cdot 4)$

In the lefthand panels of figure 12 the following interval $s = (0.9 - I \cdot 4, 0.9 + I \cdot 4)$ is displayed for five different increased values of the minimum prime in Z_C partial Euler product calculation $P_{min} = 13$ with each row (top to bottom) respectively belonging to the different α' values $\{0.1, 0.8, 0.842, 0.9, 0.99\}$.

In the righthand panels, the real and imaginary parts of the approximation error equation (50) for Z_C is displayed over the central interval of the input spectra $s = (0.9 - I \cdot 4, 0.9 + I \cdot 4)$

It can be seen from figures 11 and 12 that for the interval $t=(-4,4)$ (using fourier analysis of $\sim 150,000$ points in the interval $t=(-750,750)$)

- (i) For small or large α' values $\{0.1, 0.99\}$ the real (imaginary) parts of the approximation error equation (50) is absorptive (dispersive).
- (ii) $\alpha' \sim 0.842$ has the smallest approximation error when $\sigma = 0.5$ and the $0.842 < \alpha' < 0.9$ has the smallest approximation error when $\sigma = 0.9$ where the error lineshape is approaching $O\left(\left(\frac{1}{(s-1)}\right)^2\right)$ behaviour

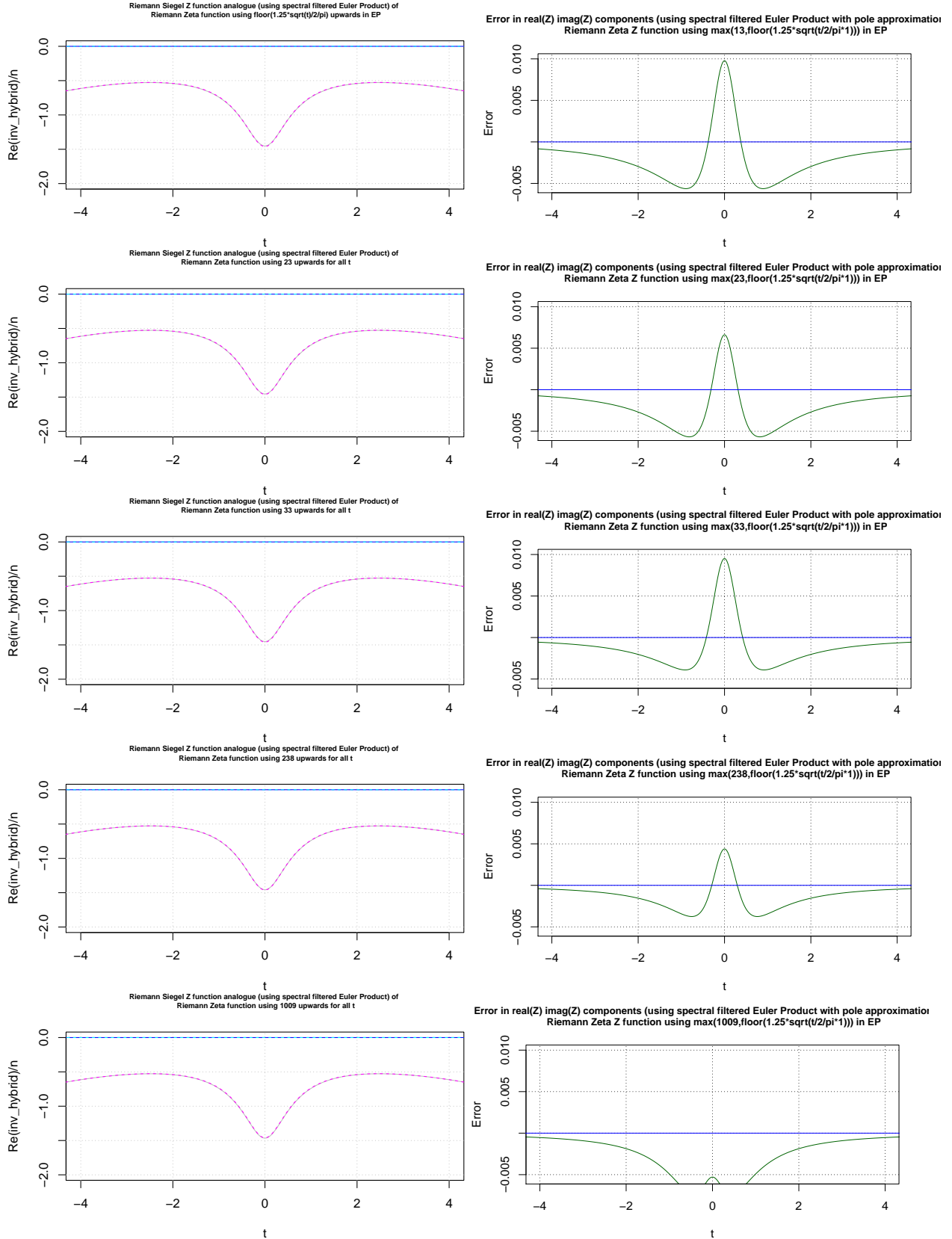


Figure 10: Lefthand panel - True Z function shown in magenta (cyan) for real (imaginary) parts and spectral filtered based EP approximation shown in gray (blue) for real (imaginary) parts, Right hand panel - Error in the real(Z) darkgreen imag(Z) blue EP approximation. A comparison of the Riemann-Siegel Z function of the Riemann Zeta L-function²³ and spectrally filtered partial Euler Product (using truncation at $\max(P, 1.25 \cdot \sqrt((\frac{|t|}{2\pi})^1 \cdot 1))$) in the complex plane at $\sigma = 0.5$ for the interval $t=(-750,750)$ where $P_{min} = 13, 23, 33, 238, 1009$ for rows 1-5. The approximation error around $t=0$ does not disappear by adding primes.

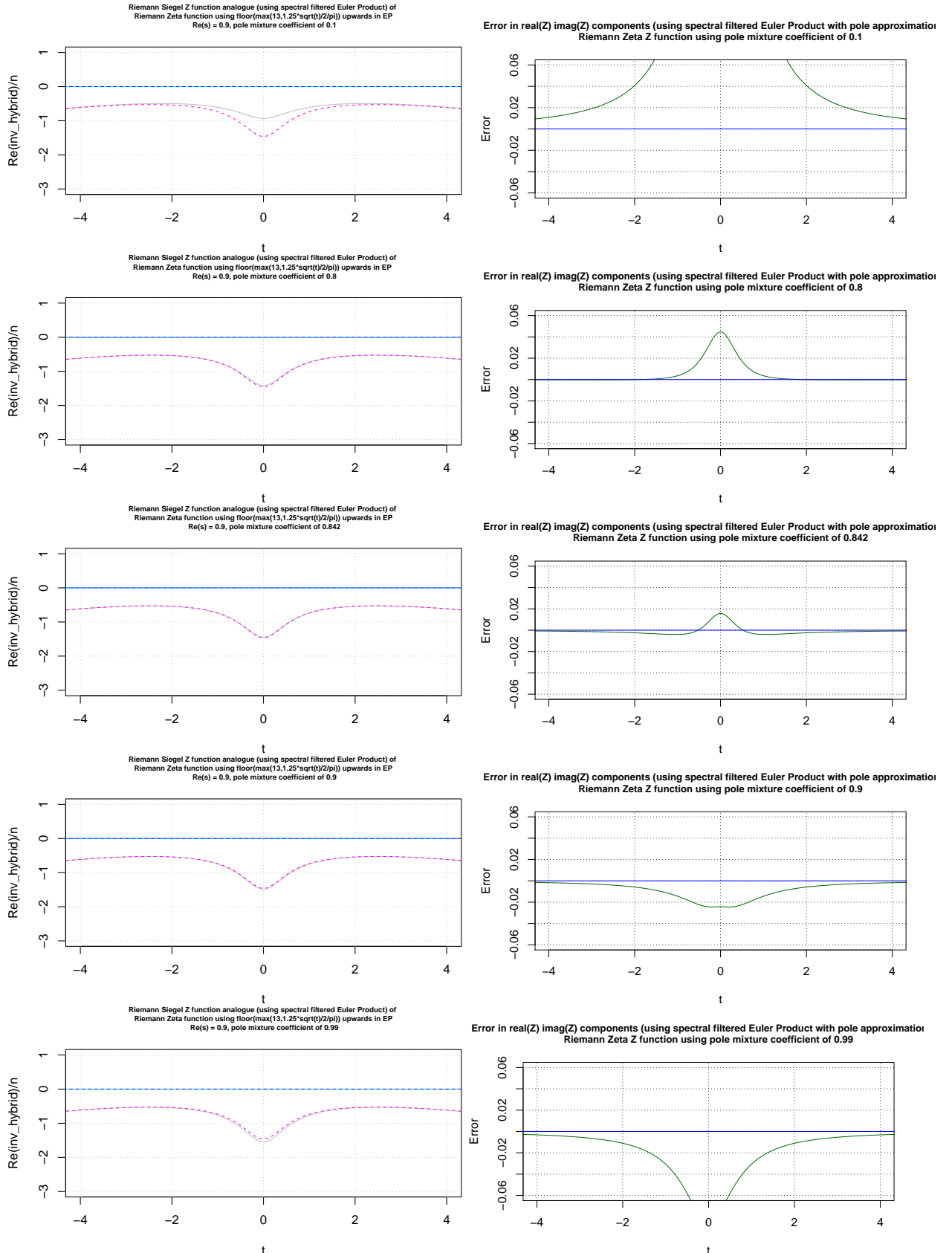


Figure 11: Lefthand panel - True Z function shown in magenta (cyan) for real (imaginary) parts and spectral filtered based EP approximation shown in gray (blue) for real (imaginary) parts, Right hand panel - Error in the real(Z) darkgreen imag(Z) blue EP approximation. A comparison of the normalised Riemann-Siegel Z function of the Riemann Zeta L-function and spectrally filtered partial Euler Product using truncation at $P=13$ in the complex plane at $\sigma = 0.5$ for the interval $t=(-750,750)$ where the pole linear combination coefficient is $\{0.1, 0.8, 0.842, 0.9, 0.99\}$ for rows 1-5.

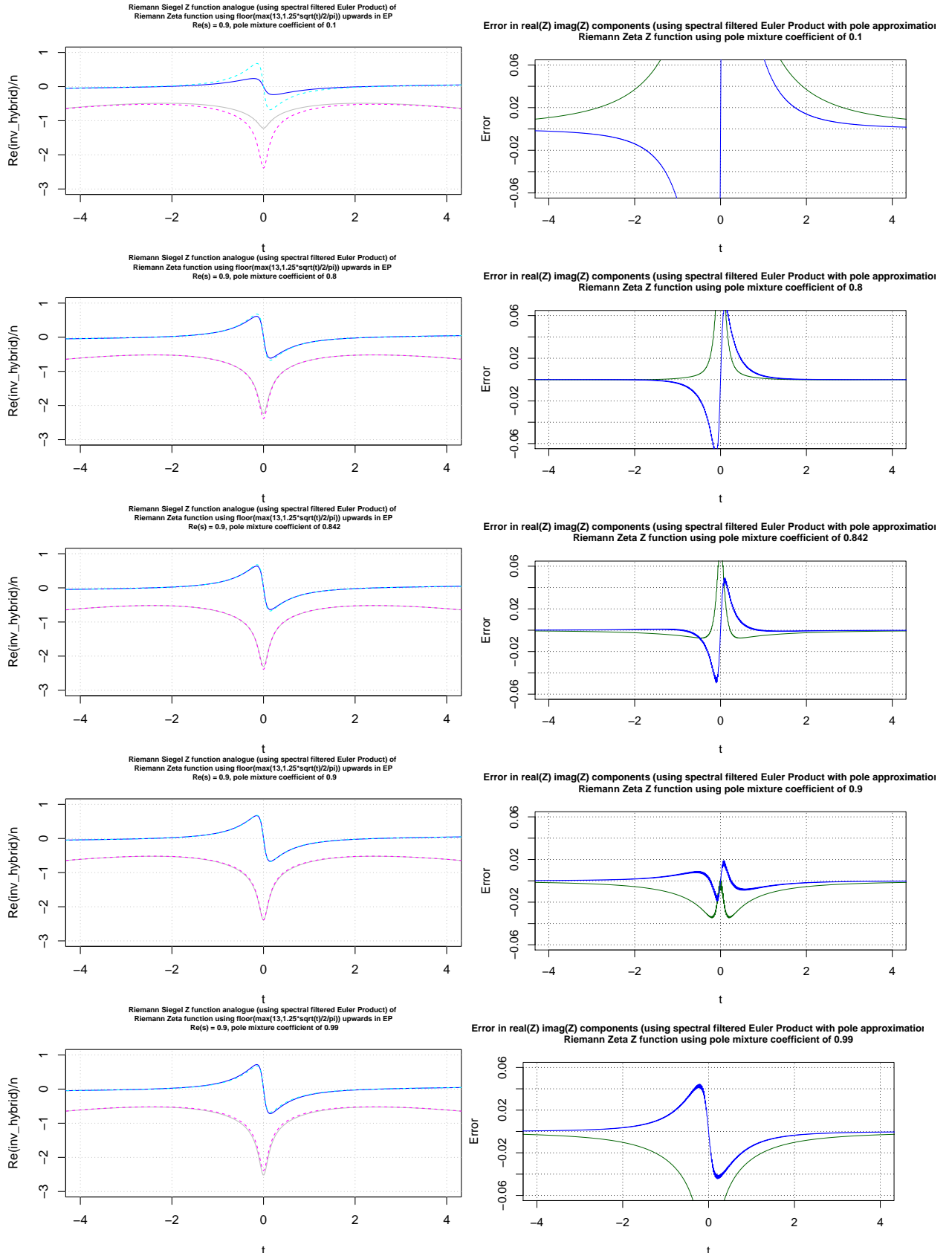


Figure 12: Lefthand panel - True Z function shown in magenta (cyan) for real (imaginary) parts and spectral filtered based EP approximation shown in gray (blue) for real (imaginary) parts, Right hand panel - Error in the real(Z) darkgreen imag(Z) blue EP approximation. A comparison of the normalised Riemann-Siegel Z function of the Riemann Zeta L-function and spectrally filtered partial Euler Product using truncation at $P=13$ in the complex plane at $\sigma = 0.9$ for the interval $t=(-750,750)$ where the pole linear combination coefficient is $\{0.1, 0.8, 0.842, 0.9, 0.99\}$ for rows 1-5.

Conclusions

Robust spectrally filtered based partial Euler Product approximation of the Riemann-Siegel Z function of the Riemann Zeta L-function within the critical strip around the real axis requires modification of the Riemann-Siegel formula (i) to use the normalised Riemann-Siegel Z function definition and (ii) inclusion of explicit pole terms in the input spectra to be fourier analysed and spectrally filtered. In practice both the partial Euler Product and the pole terms contribute to the total function behaviour on the real line of the pole.

References

1. Martin, J.P.D. "A useful approximation of the Riemann Zeta function away from the real axis using spectral filtering of the partial Euler product" (2025) <http://dx.doi.org/10.6084/m9.figshare.28528652>
2. Martin, J.P.D. "Crucial steps for robust first quiescent region truncated partial Euler Product based approximations of closely spaced Riemann Zeta function non-trivial zeroes" (2025) <http://dx.doi.org/10.6084/m9.figshare.29095232>
3. Martin, J.P.D. "Examples of spectrally filtered first quiescent region truncated partial Euler Product based approximations of Riemann Siegel Z functions for different L-functions and the two Davenport-Heilbronn 5-periodic functions on the critical line away from the real axis" (2025) <http://dx.doi.org/10.6084/m9.figshare.29577545>
4. Martin, J.P.D. "For L-functions without poles spectrally filtered first quiescent region truncated partial Euler Product based estimates of Riemann-Siegel Z functions can provide useful standalone approximations about the real axis across the critical strip." (2025) <https://dx.doi.org/10.6084/m9.figshare.29825609>
5. Edwards, H.M. (1974). Riemann's zeta function. Pure and Applied Mathematics 58. New York-London: Academic Press. ISBN 0-12-232750-0. Zbl 0315.10035.
6. Riemann, Bernhard (1859). "?ber die Anzahl der Primzahlen unter einer gegebenen Gr?sse". Monatsberichte der Berliner Akademie.. In Gesammelte Werke, Teubner, Leipzig (1892), Reprinted by Dover, New York (1953).
7. Titchmarsh, E.C. (1986) The Theory of the Riemann Zeta Function. 2nd Revised Heath-Brown, D.R.) Edition, Oxford University Press, Oxford.
8. The LMFDB Collaboration, The L-functions and Modular Forms Database, <http://www.lmfdb.org>
9. Berry, M. V. "The Riemann-Siegel Expansion for the Zeta Function: High Orders and Remainders." Proc. Roy. Soc. London A 450, 439-462, 1995.
10. J. Arias De Reyna, "High precision computation of Riemann's Zeta function by the Riemann-Siegel formula", Mathematics of Computation Vol 80, no. 274, 2011, Pages 995–1009
11. The PARI~Group, PARI/GP version 2.12.0, Univ. Bordeaux, 2018, <http://pari.math.u-bordeaux.fr/>.
12. R Core Team (2017). R: A language and environment for statistical computing. R Foundation for Statistical Computing, Vienna, Austria. <https://www.R-project.org/>.
13. RStudio Team (2015). RStudio: Integrated Development for R. RStudio, Inc., Boston, MA <http://www.rstudio.com/>.